Original Research Article

# Novel shearhead reinforcement for slab-column connections subject to eccentric load and fire

*Rwayda Kh. S. Al-Hamd* [a,b,*], *Martin Gillie* [c], *Lee S. Cunningham* [a],
*Holly Warren* [d], *Asad S. Albostami* [a]

[a] *School of Mechanical, Aerospace and Civil Engineering, The University of Manchester, Manchester M13 9PL, UK*
[b] *Al-Nahrain University, Baghdad, Iraq*
[c] *The School of Engineering, The University of Warwick, Coventry, CV4 7AL, UK*
[d] *International Paint Ltd, Stoneygate Lane, Felling, Gateshead, Tyne and Wear, NE10 0JY, UK*

**ABSTRACT**

Traditional means of reinforcing concrete flat slab-column connections against punching shear, such as increasing slab thickness, or provision of shear links, all have drawbacks. This paper proposes a novel type of punching shear reinforcement in the form of a shearhead to enhance connection strength and ductility. The structural behaviour of the connection is explored experimentally by testing nine specimens under various loading conditions including eccentric loads that produce combined axial and bending effects. Specimens with and without shearheads are compared. This is followed by a detailed numerical investigation using finite element analysis to obtain more in-depth insights into the connection behaviour when shearheads are present. The performance of the proposed system is also investigated under fire conditions for the first time. It is found that the proposed shearheads improve the performance of slab-column connections in all conditions and particularly under concentric loading and in fire conditions.

## 1. Introduction

Flat slab structures are a type of construction where a concrete floor plate is connected directly to columns without the presence of beams, as such, they are the simplest form of a reinforced concrete frame (Fig. 1a). They are advantageous due to the construction work savings, aesthetically pleasing appearance and elimination of beams and girders which allows t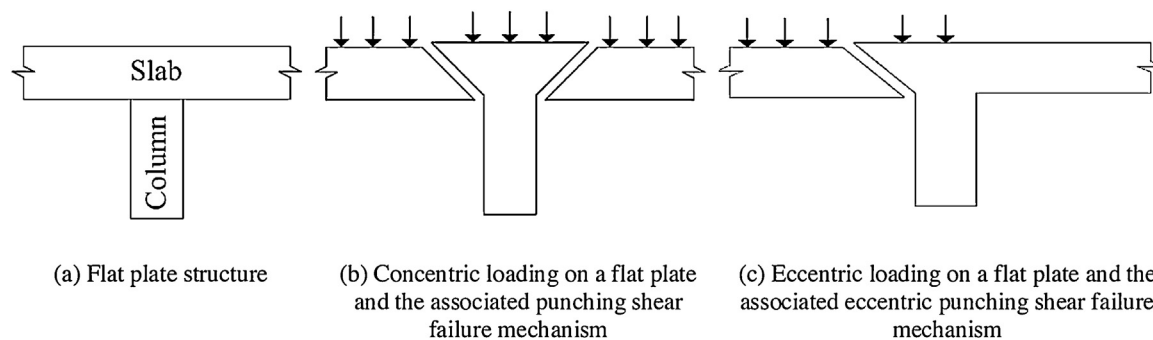he overall floor depth in multi-storey buildings to be reduced, thus creating extra floor space for a given building height [1]. However, in this type of structure slab-column connections can be subject to simultaneous large shear forces and bending moments. This kind of load scenario typically results in two failure modes, the most common is when the column punches through the slab and causes "symmetrical punching shear". The second mode is when the bending moments affect the loading, i.e. when the floors are not loaded equally, causing "un-symmetrical punching shear". These types of failure are shown in Fig. 1b and c, respectively. In both

---

(a) Flat plate structure

(b) Concentric loading on a flat plate and the associated punching shear failure mechanism

(c) Eccentric loading on a flat plate and the associated eccentric punching shear failure mechanism

**Fig. 1 – Schematic diagram of a flat slab reinforced-concrete structure.**

cases failure is brittle and sudden, consequently punching shear is dangerous and has been the subject of previous and ongoing research. There have been several structural failures in recent times due to punching shear, some resulting in the wholesale collapse of buildings [2].

Many studies propose ways to enhance the slab-column connection such as using high-strength concrete, steel fibre reinforced concrete and more traditionally shear reinforcement in the form of links or stirrups [3]. In many cases, the shear reinforcement can be expensive both financially and in terms of construction time, and can be difficult to install. In this paper, the behaviour of a novel form of shearhead reinforcement is investigated. Both experimental tests and numerical models are conducted to investigate the capability of this kind of reinforcement. A shearhead is a structural member embedded at the slab-column connection. The main advantage of shearheads is that they distribute the load of the floor on the respective columns and reduce the effect of the vertical force, i.e. they spread the critical section away from the columns resulting in a large shear perimeter around the column and higher punching shear resistance.

Experimental testing is undertaken to prove that the shearheads are sufficient for both the effects of concentric and eccentric loads. Eccentric loads may occur for a range of reasons. Such loading scenarios are common in (relatively lightly loaded) edge and corner columns, however, pattern loading can produce moments in more heavily loaded interior columns, and the effects of fire can be similar.

## 2. Background and previous studies

The idea of flat slabs was developed in the USA in the early twentieth century and was initially used for footings rather than floor plates. Turner [4,5] was most influential in developing flat slab structures during the period 1905–1909, which were called "mushroom head" structures by engineers at the time, due to the inclusion of a local larger column diameter at the slab-column connection. Turner's work was reported by Gasparini [4] who proved that the mushroom head concept introduced by Turner was economically efficient and reliable for both buildings and bridges.

Talbot [6] in 1913 tested column footings and provided an early basis for punching shear design. However, tests of the punching shear resistance of floor slabs (rather than founda-

tions) came relatively late with the work of Elstner and Hogestad [7] being the first major study. This was followed by the work of Moe [8], which resulted in the early ACI code [9] for punching shear. All these early tests were conducted with solely concentric forces; no moments were applied to the slab-column connections. Ghoreish et al. [9] and Hamada et al. [10,11] provide a detailed review of punching shear experiments.

The early tests focused on concentric loading conditions until around the 1970s when Hawkins and Corley [12], and later Islam and Park [13,14] examined the effects moments had on slab-column connections. These authors produced moments by applying lateral forces on one side of the column. Several later researchers followed this approach to applying moments including Melgabry and Ghali [15], Kang et al. [16], Moreno and Sarmento [17] and Song et al. [18]. Kruger et al. [16]. proposed a new method for applying moments in punching shear tests, by applying an eccentric column load through an offset corbel [19,20] (Fig. 4 shows a similar setup). Their main finding was that the presence of a moment significantly decreased the resistance of slabs to punching shear, which is in line with earlier findings [12,14]. The experiments described in the present paper adopt Kruger's method of applying loads together with moments to the slab-column connection. The benefit of this method is that only one loading device is needed.

Different strategies were proposed by researchers to enhance the slab-column connection as mentioned previously. The simple concept of shearheads was suggested by Moe in 1961 [8] by embedding a steel plate at the column-slab connection (shown in Fig. 2a). In Moe's work, three thick slabs were tested in which the steel plates were intended to increase the effective size of the column. However, the steel plates did not add much shear resistance. Corley and Hawkins [10,12] investigated shearhead reinforcement in more detail, by performing 21 tests, 16 of which contained a grillage of I and Channel sections, as shown in Fig. 2b and c. The results of these tests were used to develop the ACI [21] shearhead design criteria for interior column locations. The tests showed that once inclined cracking forms in the slab adjacent to the connection, all subsequently applied shear is carried by the shearhead. Failure is initiated either by punching along a surface following the perimeter of the shearhead or by reaching the flexural capacity of the shearhead at the column face. The present paper researches an economic novel shear-
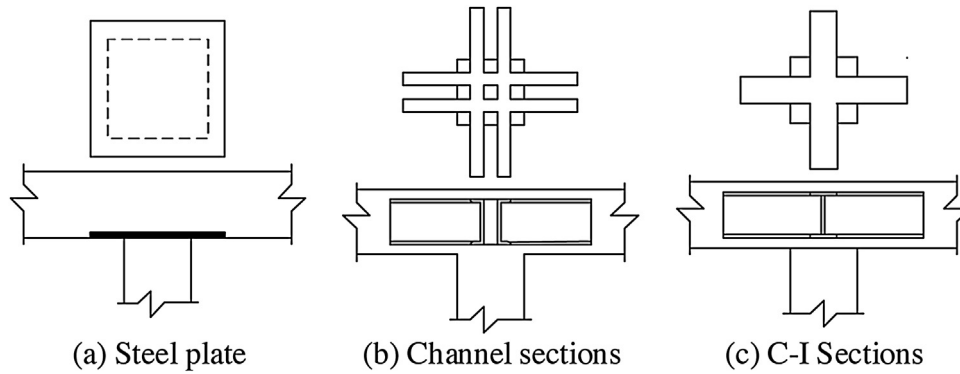
(a) Steel plate          (b) Channel sections          (c) C-I Sections

**Fig. 2 – Types of shearhead reinforcement.**

head type, which was proposed by the underlying assumption for load carrying mechanisms suggested by both Moe and Corley and Hawkins [10,12].

Attempts to numerically model punching shear behaviour have been limited under eccentric and fire loading, possibly due to the difficulties in accurately capturing the behaviour of reinforced concrete numerically. The available studies include work by Polak et al. [22,23] for slab-column connections under concentric loading. Polak et al. were able to detect the stress and strain states induced by punching behaviour, but were not able to predict failure loads. Their main finding was that it was possible for the concrete model to simulate the experiment and to capture the cracking pattern with a relative error of $\pm15.06$–20.07%. A recent study by Abdulrahman et al. in 2017 [24] used the same approach proposed by Polak et al. [22,23] to model corner slab-column connections. In this study, the relative error was reduced to between $\pm1.01$ and 11.20%. To date, it appears that limited numerical studies investigate punching shear with eccentric loads.

Considering this background, this paper focusses on three items. Firstly, the behaviour of the novel shearhead system from a series of experiments is presented. Secondly, a detailed numerical model is developed, validated and subsequently used to obtain a deeper understanding of the proposed reinforcement system. Lastly, the numerical model, is used to explore the behaviour of the reinforced slab system in fire conditions. The aforementioned represents the first such study of this kind of shearhead system in fire.

## 3. Shearhead system design concept

The design of the shearhead system discussed in this paper was based on the combination of two novel ideas. The first was proposed by Moe [8], who developed an elementary shearhead system that enhances punching shear resistance by placing a steel plate at a minimum distance of $d/2$ from the column face. The second was developed by Corley and Hawkins [10,12], who suggested the use of an I-shaped or Channel-shaped section placed at a distance from the column face to ensure a wider area of stress distribution under the load. The present study brings together the advantages of the two approaches. This was achieved by fabricating a novel shearhead design which consists of a steel section extending 1.25 × slab depth either side of the column face to ensure that the shearhead would develop a resistance to the cracking path (the shearhead schematic is shown in Fig. 3).

## 4. Experimental setup and programme

The experimental work presented in this paper consists of testing nine specimens. All the specimens were scaled to approximately 1/3 of the size of a typical practical flat slab. The specimens were designed to exhibit punching shear behaviour with and without shearheads. Varying amounts of eccentric loading were applied, allowing the effect of increasing the
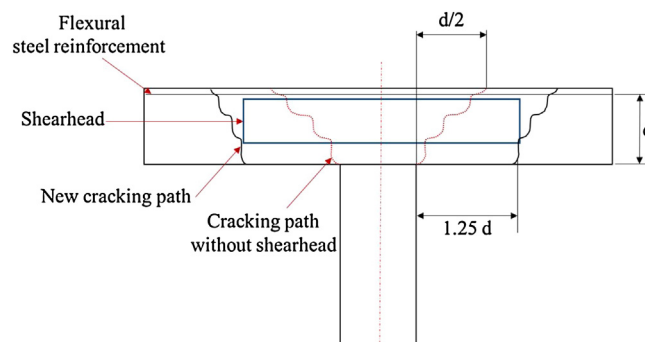


**Fig. 3 – Conceptual drawing demonstrating the effect of adding shearhead reinforcement.**

**Table 1 – Tested specimens.**

| Group | Slab designation | Eccentricity, e [mm] | Punching reinforcement |
|---|---|---|---|
| G1 | S0 | 0 | None |
|  | S60 | 60 |  |
|  | S120 | 120 |  |
| G2 | SHS0 | 0 | Shearhead (28 cm × 28 cm) |
|  | SHS60 | 60 |  |
|  | SHS120 | 120 | With Single cross stiffener |
| G3 | SHD0 | 0 | Shearhead (28 cm × 28 cm) |
|  | SHD60 | 60 |  |
|  | SHD120 | 120 | With double cross stiffeners |

slab-column connection bending moment on the failure mode to be investigated. Table 1 shows the specimen details.

The test specimens were geometrically identical (dimensions shown in Fig. 4) and consisted of a square slab area designed to simulate an area of floor plate and a corbel. The corbel was designed to allow eccentric loading to be applied and to represent a column attached to a floor plate. This experimental set-up was similar to that used by [20]. Flexural reinforcement consisting of mesh amounting to a 1% reinforcement ratio (in both directions) was provided in all the specimens to ensure a shear failure mode. The columns and corbels were reinforced with seven 12 mm bars evenly spaced with 15 mm cover and 6 mm links in order to prevent local failure of the column. All reinforcing bars had a yield strength of 400 MPa.

Six out of the nine tested specimens had shearhead reinforcement embedded in them. The novel shearhead proposed in this paper has two different designs. Both of them consist of channel-shaped steel (C-section) welded at the corners and tee shaped steel sections. The tee shape sections were cut from I sections to make the stiffeners of the shearheads, the parent steel had a 540 MPa yield strength. Fig. 5 shows the proposed shearhead layout, and Fig. 6 shows the position of the shearhead before casting.

For practical reasons, the test set-up was inverted, hence the corbel was on the top side of the slab and the load was applied downwards (Figs. 7 and 8). Fig. 8 shows the test setup support conditions and loading frame. The slab was held at the corners using wooden blocks (50 × 100 mm) to prevent vertical movements. The wooden blocks were held down using steel rods. The slab edges were supported by the steel rods that were welded to a stiff steel frame, thus providing pinned support conditions.

The concrete mix used for all specimens had a nominal compressive cylinder strength of 26 MPa at 28 days, the time at which the slab testing took place. The concrete mix design is shown in Table 2. In addition to compressive mechanical tests, split tensile and flexural tests were also conducted on concrete specimens according to ASTM [25]. Further details of the concrete properties determined from the control specimens are given in: Mix Design.

Table 3 A local silicate aggregate was used with a maximum size of 10 mm.

The tests were undertaken in a universal hydraulic machine with 300-tonne capacity. The load was applied in 5 kN increments. The load was applied to the column via a steel loading cap, with the support frame providing a reaction. This form of loading is a close approximation to the typical in-service load on the flat slab system and was able to produce punching shear failure reliably. The loads were exerted on the loading cap via a wedge plate that was positioned at 0, 60 and 120 mm from the centre line of the column, depending on the degree of eccentricity desired. This method of providing combined axial loads with bending moments is novel as shown in Fig. 9a–c.

Deflection measurements were taken at several locations in each test as shown in Fig. 10. Dial gauges of 0.01 mm sensitivity were mounted on a steel frame, four below the slab (tension face) and one above the slab (compression face). The applied loads were measured directly from the loading machine. After slab failure, the failure angle of punching shear was noted.

## 5. Experimental results

Table 4 shows the key results, which illustrate the effect of eccentricity on both the load at first cracking and the ultimate capacity of the slabs. The first column divides the slabs into three different groups. Group G1 consists of the three slabs
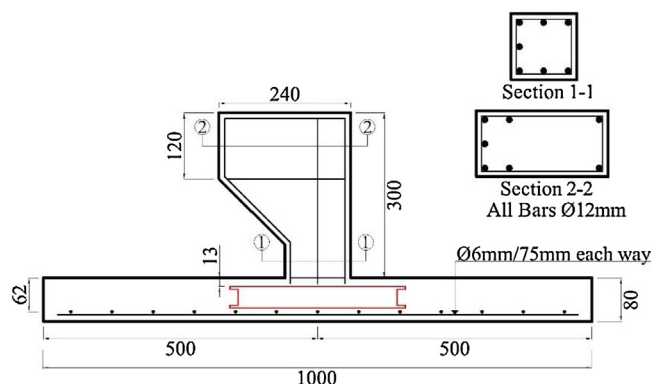


**Fig. 4 – Tested slab geometry (all dimensions in mm).**
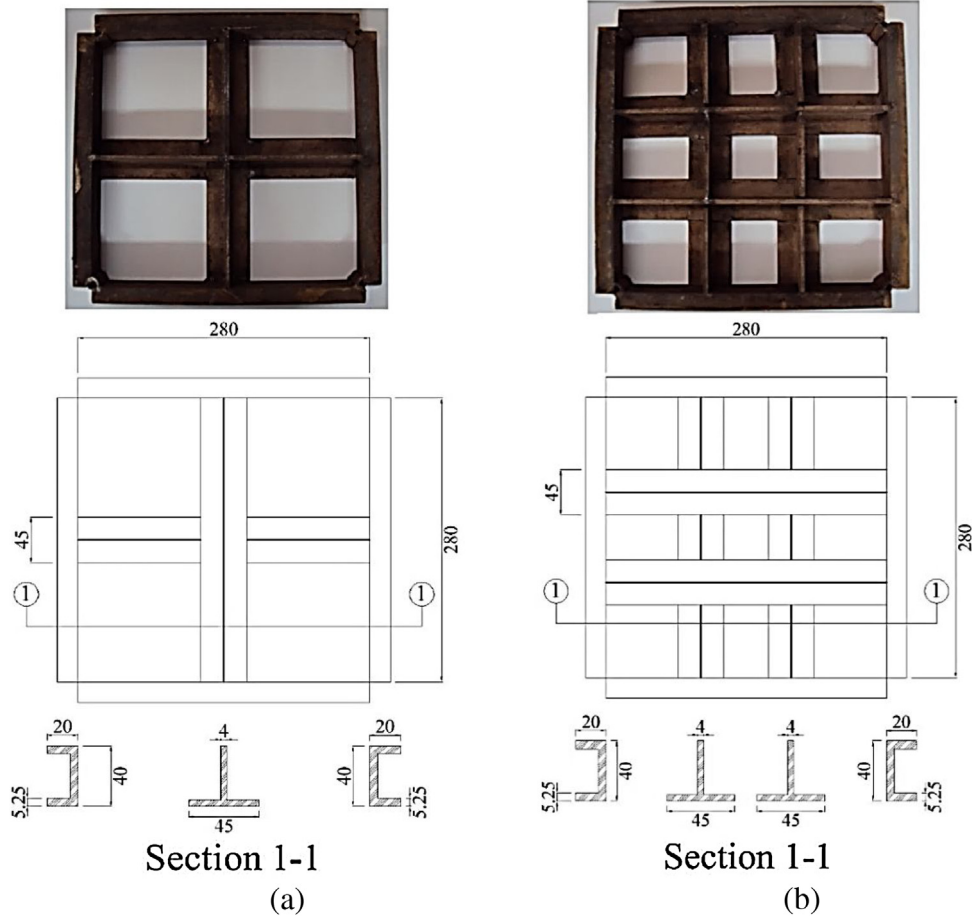
Fig. 5 – Proposed shearhead layout (a) for G2 shearhead and (b) for G3 shearhead.



Fig. 6 – Shearhead position in the slab.



Fig. 7 – Loading frame and a typical slab.

without shear reinforcement, group G2 denotes slabs with a single stiffener shear reinforcement and group G3 denotes slabs with double stiffener shear reinforcement.

As the eccentricity increases within each group, both the first cracking and ultimate load values are reduced, which is in line with earlier test results [19]. The failure mechanism as

determined by examining the crack pattern close to failure is shown in the type of failure column; with ''unsymmetrical punching'' indicating that a shear failure was observed on one side of the column but not on the other. Once the load on first cracking had been exceeded, flexural cracks started to gradually develop in each slab, until the column suddenly
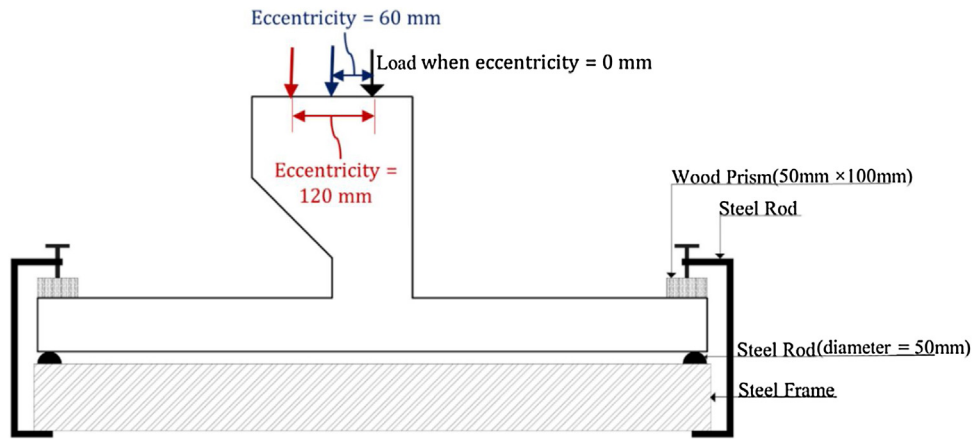
**Fig. 8 – Support conditions and loading frame.**

**Table 2 – Mix design.**

| W/C ratio | Mix proportions (kg/m³) | | | | 28 day compressive strength (MPa) | |
|---|---|---|---|---|---|---|
| | Water | Cement | Sand | Gravel | $f_c$<br>Cylinder compressive strength | $f_{cu}$<br>Cube compressive strength |
| 0.45 | 180 | 400 | 600 | 1200 | 26 | 36 |

**Table 3 – Control specimen results after 28 days (average of three control specimens for each case).**

| | | |
|---|---|---|
| Cylinder compressive strength ($f_c$) | (MPa) | 26 |
| Cube compressive strength ($f_{cu}$) | (MPa) | 34.4 |
| Modulus of elasticity ($E_c$) | (GPa) | 24 |
| Tensile strength ($f_{st}$) | (MPa) | 3.4 |

failed in full symmetrical or unsymmetrical punching shear. The increase of ultimate load in G2 and G3 compared to G1 is caused by the additional shearhead reinforcement which increases the critical shear perimeter of punching shear in the slabs. Using shearheads with double stiffeners (as in G3) gives a higher ultimate load capacity than a single cross stiffener (as in G2), because the load is distributed across more of the tension steel area.

Unsymmetrical punching shear responses are also evident from the deflection profiles of the slabs, which are shown for increasing loads (and moments) in Figs. 11–13. For the eccentric load cases, the deflection profiles become increasingly asymmetric due to the presence of the moment at the connection. Load-deflection curves for the central point of each slab are shown in Figs. 18 and 19. The slab with shearheads tends to mitigate the effects of eccentricity, producing a more symmetrical deflection profile indicating a degree of redistribution (Fig. 14).

Table 5 presents key details of the punching shear cones which were assessed after failure for each test. Shear crack angles and failure perimeters are given in each case and the critical perimeter (CP) used in various design codes (discussed in full below). Increased eccentricity decreases the critical section of the punching shear perimeter and makes the punching shear surface unsymmetrical due to the moment applied by the eccentric loading. It was found that the shearhead (in all cases) increases the critical section perimeter. This is attributed to the inclined cracks that develop first
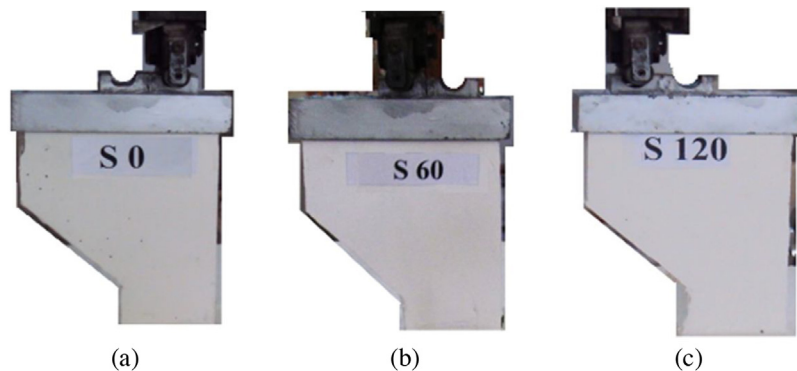


(a)                     (b)                     (c)

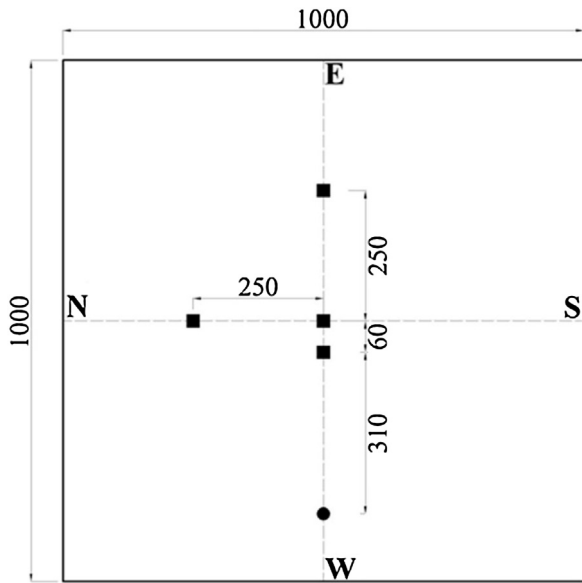**Fig. 9 – Loading arrangements for eccentricity of (a) 0 mm, (b) 60 mm and (c) 120 mm.**

**Fig. 10 – Plan layout of dial gauges and slab directions.**

along the column corner and then extend laterally. Due to the presence of the shearhead, most of these cracks will move outside the shearhead (Fig. 15).

## 6. Numerical modelling

The general-purpose finite element analysis software, Abaqus v.6.13, was used to analyse the slab-column connection. The choice of the element type, material model and model geometry are discussed in this section. A wide range of material elements is available in the Abaqus library, such as continuum (solid) elements, membrane elements, truss elements, beam elements, shell elements and special purpose elements [26].

There are two broad methods of modelling slab-column connections used by researchers: one is by using 3-D continuum (solid) elements to model the concrete and truss elements to model the reinforcement mesh and bars. This approach was first adopted by Winkler [27]. The other approach was suggested by Gorge and Tian [28] and uses shell elements for the slab, with rebar represented as a 'layer' of steel within the shells. The numerical models in this project used 3-D solid elements (C3D8R) [26] to represent the concrete slab, with truss elements (T3D2) embedded within them to represent the rebar. This approach has a number of advantages such as providing a better representation of the complex 3-D stress state that exists near the slab-column interface under punching shear, capturing the shear stresses in the connection. However, solid elements are not good at modelling bending behaviour [29]. Commonly, quite a fine thickness of mesh is required to capture bending strain accurately. This requirement conflicts with the need for a mesh size comparable with the largest aggregate size in concrete if finite element models are to capture the complex softening behaviour that reinforced concrete exhibits [30]. For this reason, shell element models were also produced in order that results could be compared.

For concrete modelling, the concrete damaged plasticity (CDP) model is a plasticity model that considers both tensile cracking and compressive crushing of concrete as possible failure modes. Therefore, it can be described as a damage-based model. The CDP model showed its accuracy in modelling all the types of concrete structures for both plain and reinforced concrete at both high and low confining pressures. This model was first developed by Lubliner et al. [31]. The main components of the CDP model are the yield function, the flow rule and the hardening rule. Lubliner et al. [31] in 1989 developed a yield function for the constitutive model. The yield function was enhanced by Lee et al. [32] in 1998, introducing fracture energy damage and stiffness degradation.

The CDP model described in the preceding section was used to model the concrete where the uniaxial compressive stress-strain relationship was adopted from Eurocode 2 [33] and uniaxial tension behaviour was adopted from Wang and Hsu [34], after a validation study. CDP input parameters are shown in Table 6; eccentricity, yield surface (Kc) and viscosity values were obtained from the literature as explained in the previous section, and the dilation angle and the ratio of initial equibiaxial compressive yield stress to initial uniaxial compressive values were chosen after calibrating the model.

The applied load was introduced to the model through a loading plate, to simulate the experiment, with an appropriate degree of eccentricity according to the test, no symmetry boundary conditions were used.

The aggregates used in the experimental work had a maximum size of 10 mm. Since the macroscale behaviour of concrete depends on aggregate size, the mesh size needed to

| Table 4 – Experimental results. | | | | | |
|---|---|---|---|---|---|
| Group | Slab designation | Cracking load (Pcr) (kN) | Ultimate load (Pult) (kN) | Ultimate moment (Mult) (kN.m) | Type of failure |
| G1 | S0 | 26.3 | 74.0 | 0.00 | Symmetrical punching |
| | S60 | 20.0 | 71.5 | 4.29 | Symmetrical punching |
| | S120 | 17.5 | 65.8 | 7.89 | Unsymmetrical punching |
| G2 | SHS0 | 27.5 | 84 | 0.00 | Symmetrical punching |
| | SHS60 | 21.25 | 77 | 4.62 | Unsymmetrical punching |
| | SHS120 | 18.75 | 72.5 | 8.70 | Unsymmetrical punching |
| G3 | SHD0 | 30 | 96.5 | 0.00 | Symmetrical punching |
| | SHD60 | 25 | 89 | 5.34 | Symmetrical punching |
| | SHD120 | 20 | 85.75 | 9.75 | Unsymmetrical punching |

(a) Slab S0

(b) Slab S60

(c) Slab S120
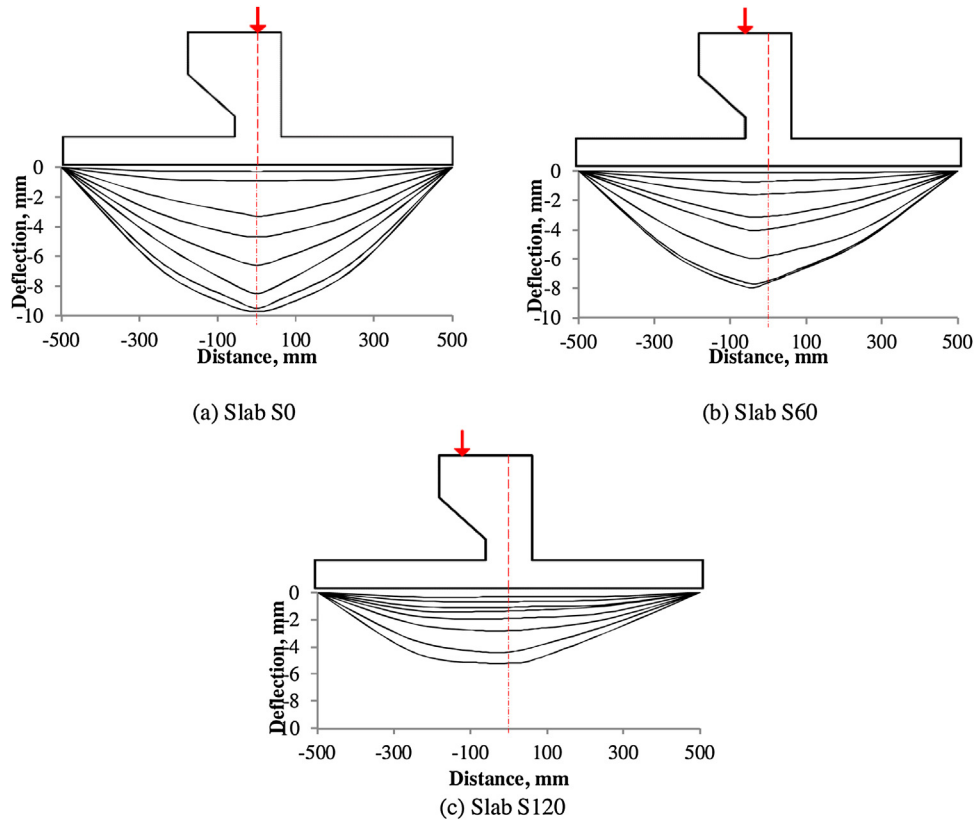
**Fig. 11 – Deflection profile in N-S direction for G1 (5 kN load increments).**



(a)  Slab SHS0

(b)  Slab SHS60

(c) Slab SHS120
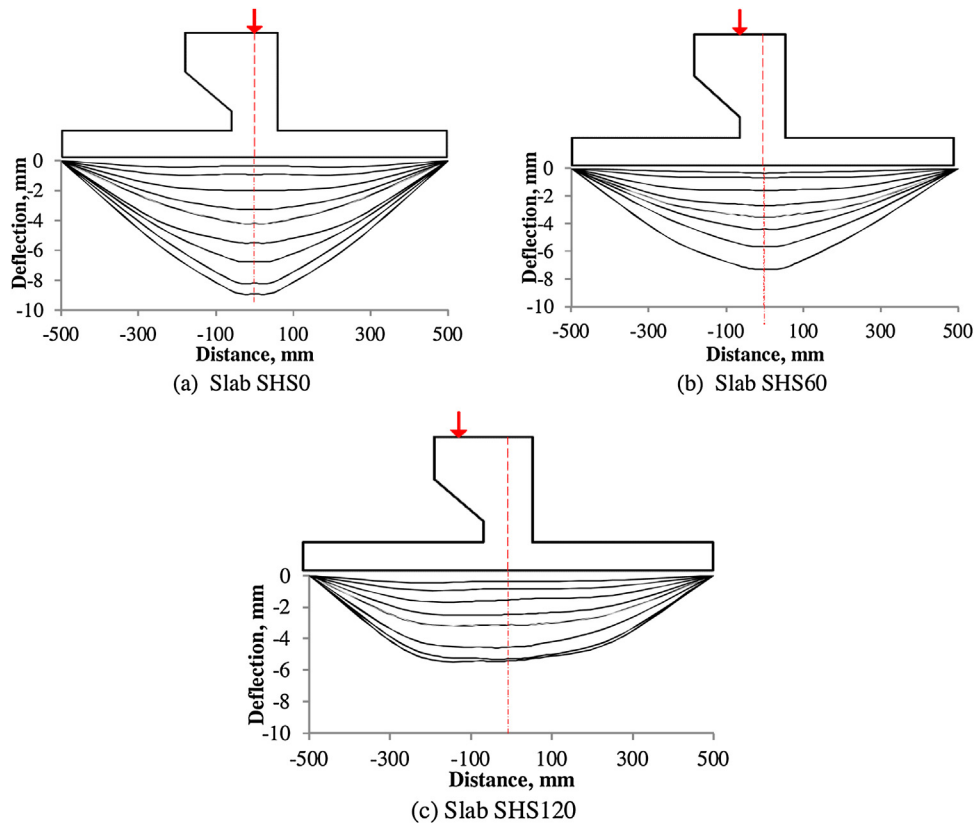
**Fig. 12 – Deflection profile in N-S direction for G2 (5 kN load increments).**
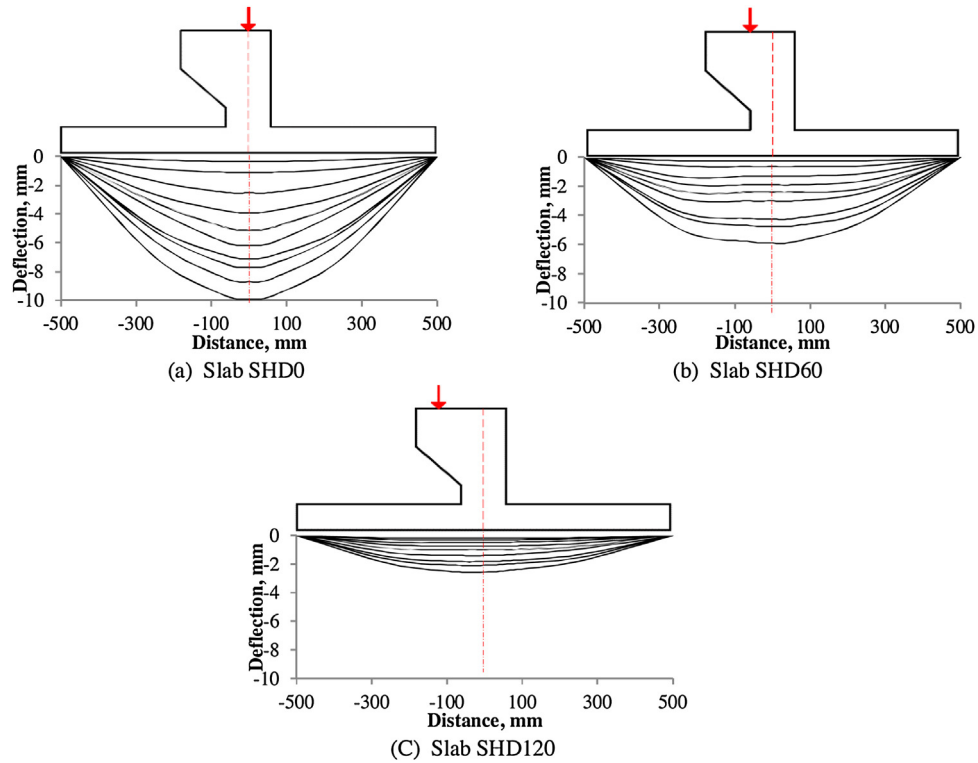
(a) Slab SHD0

(b) Slab SHD60

(C) Slab SHD120

**Fig. 13 – Deflection profile in N-S diection for G3 (5 kN load increments).**
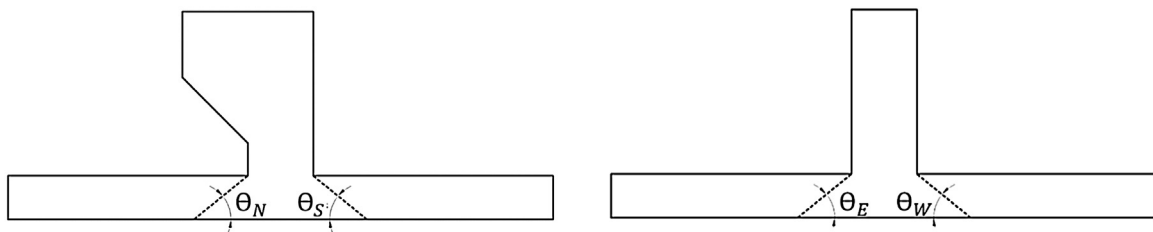


**Fig. 14 – Location of failure angles.**

| Table 5 – Failure perimeters and failure angles. | | | | | | |
|---|---|---|---|---|---|---|
| Group | Slab | Failure perimeter mm | ΘN° | ΘS° | ΘE° | ΘW° |
| G1 | S0 | 1336 | 17.10 | 15.70 | 15.40 | 19.90 |
|  | S60 | 1174 | 20.20 | 19.30 | 15.30 | 22.50 |
|  | S120 | 1063 | 21.70 | – | 19.20 | 15.99 |
| G2 | SHS0 | 1635 | 13.40 | 16.41 | 15.60 | 16.50 |
|  | SHS60 | 1520 | 12.50 | – | 11.79 | 12.53 |
|  | SHS120 | 1517 | 14.80 | – | 10.38 | 12.58 |
| G3 | SHD0 | 1695 | 17.67 | 16.00 | 12.78 | 12.87 |
|  | SHD60 | 1688 | 16.42 | 14.77 | 13.06 | 13.99 |
|  | SHD120 | 1455 | 14.68 | – | 13.00 | 13.97 |

be greater than the maximum aggregate size [30] for accurate results. A mesh sensitivity study (Fig. 16) showed there was no strong mesh sensitivity provided elements bigger than the aggregate size were chosen, and correspondence with the test results was good, therefore to aid computational speed, a mesh size of 20 mm was chosen for the analyses [22,23,35].

In line with previous approaches to modelling the complex tensile behaviour of reinforced concrete [34,36,37], the approach taken in this study was to introduce "tension softening" behaviour to the numerical model. A further sensitivity study was performed to identify the most appropriate form of this tension softening behaviour. Several
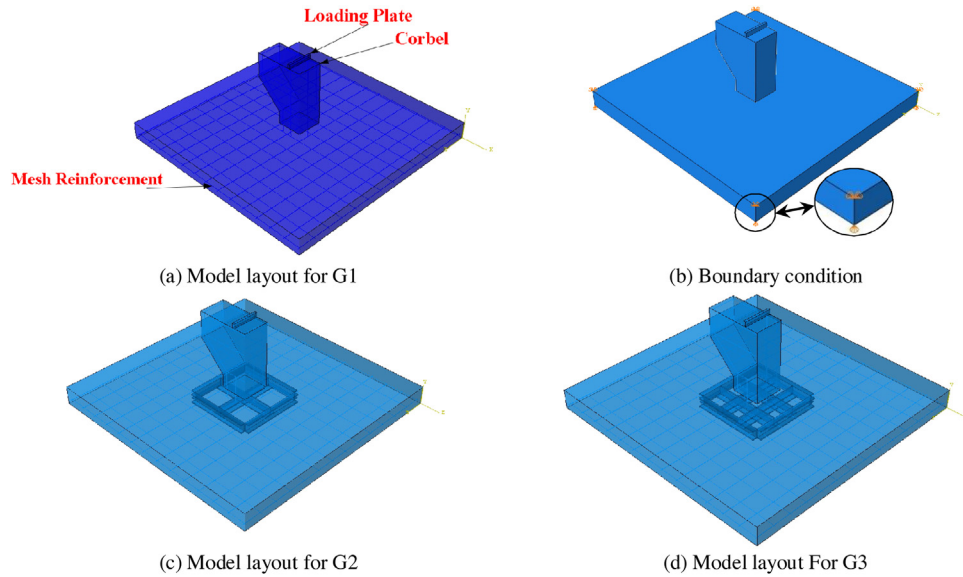
(a) Model layout for G1

(b) Boundary condition

(c) Model layout for G2

(d) Model layout For G3

**Fig. 15 – FEM details.**

**Table 6 – Parameters for concrete damage input.**

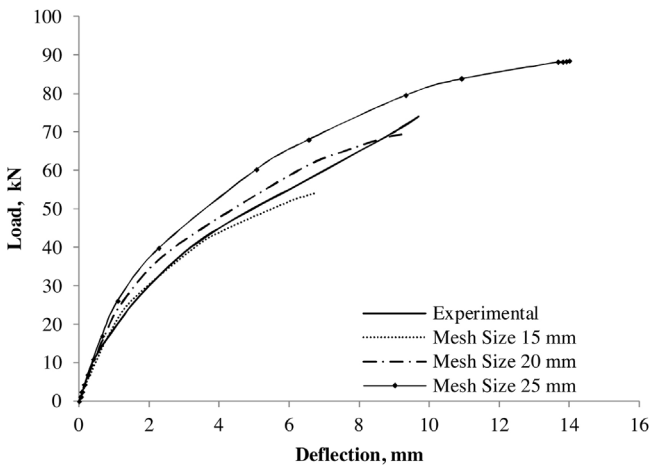| Dilation angle | Eccentricity | $\sigma_{b0}/\sigma_{c0}$ | $K_c$ | Viscosity parameter |
|---|---|---|---|---|
| 40° | 0.1 | 1.16 | 2/3 | 0 |



**Fig. 16 – Mesh sensitivity study for the S0 test.**

concrete tension models such as linear, bilinear, Hordijk's [37] and Wang and Hsu's [34] models were examined. Fig. 17 shows that linear and bilinear models give poor results while Hordijk's, and Wang and Hsu's match experimental results closely; Wang and Hsu's model was therefore used as it was slightly simpler to implement.

Abaqus offers two numerical methods to analyse nonlinear problems: a general static procedure and a Riks arc-length approach [26]. The two types of analysis were used to validate the numerical model against the experimental results presented here as shown in Fig. 18a–c. In the analyses presented, the general static solver showed its ability to predict the same

failure load as that predicted by the Riks approach. The Riks approach assumes the first peak of the load-deflection curve to represent the cracking of the concrete, leading to failure [80]. Therefore, in this study, the use of the general static solver is preferred. The models with 0, 60 and 120 mm of eccentricity showed an accuracy of 6.67, 5.03 and 7.69%, respectively as shown in Table 7. The failure mechanism is discussed in more detail in Section 7.

After validating both the material approach and the loading application, the shearheads are introduced in the model, the load versus central deflection curves are shown in Fig. 19. Load versus central deflection predictions are very close to the experiments within a relative error of between 0.73 and 6.12% as shown in Table 7. In some cases, the initial pre-failure deflection behaviour was not captured in the FE models and they show a stiffer response compared to the test due to the simple supports that are adopted; however, this does not affect the failure mechanism or the predicted failure load (see Section 7). This result provides additional validation and confidence in the numerical models presented, demonstrating that the modelling approach taken can simulate the slab-column connection behaviour both with and without shear reinforcement.

## 7. Identification of punching shear behaviour in the numerical model

Punching shear is a brittle failure resulting from complex three-dimensional stress states and interaction between concrete, rebar, cracking and other factors. Previous attempts to model punching shear have been limited to predicting
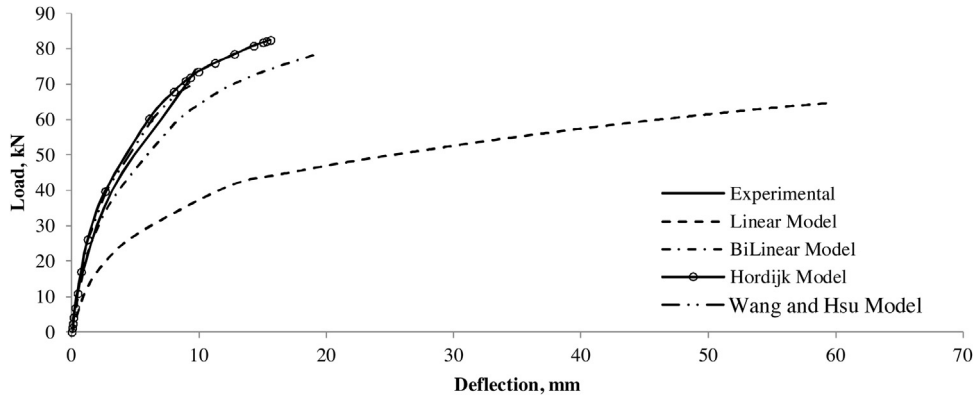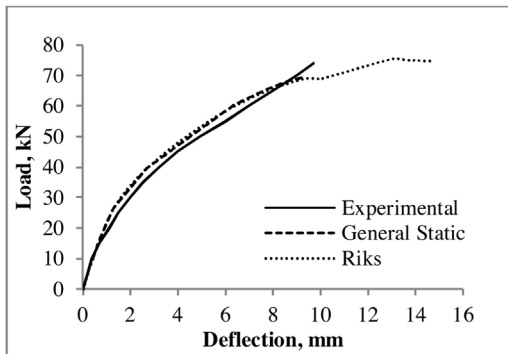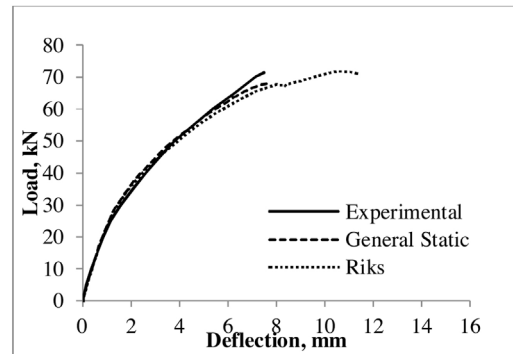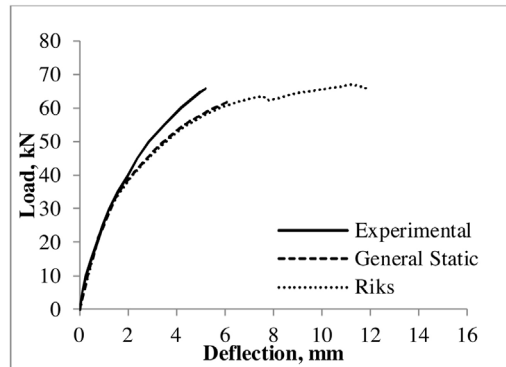
Fig. 17 – Load–central deflection curves using different tension softening models.



(a) Slab S0        (b) Slab S60



(c) Slab S120

Fig. 18 – Load–central deflection curves using different models for (a) slab S0 (b) slab S60 and (c) slab S120.

| Table 7 – The ultimate load obtained from experiments and FE model predictions. | | | | | | |
|---|---|---|---|---|---|---|
| Group | Slab designation | Ultimate load (Pult) (kN) | Ultimate moment (Mult) (kN m) | FE models (Pult) (kN) | FE (Mult) (kN m) | Relative error % |
| G1 | S0 | 74.0 | 0.00 | 69.07 | 0.00 | 6.67 |
| | S60 | 71.5 | 4.29 | 67.68 | 4.06 | 5.34 |
| | S120 | 65.8 | 7.89 | 61.10 | 7.33 | 7.14 |
| G2 | SHS0 | 84 | 0.00 | 80.30 | 0.00 | 4.41 |
| | SHS60 | 77 | 4.62 | 77.56 | 4.65 | 0.73 |
| | SHS120 | 72.5 | 8.70 | 68.99 | 8.28 | 4.84 |
| G3 | SHD0 | 96.5 | 0.00 | 101.8 | 0.00 | 5.50 |
| | SHD60 | 89 | 5.34 | 93.50 | 5.61 | 5.1 |
| | SHD120 | 85.75 | 9.75 | 91.00 | 10.92 | 6.12 |

(a) slab SHS0

(b) slab SHS60

(c) slab SHS120

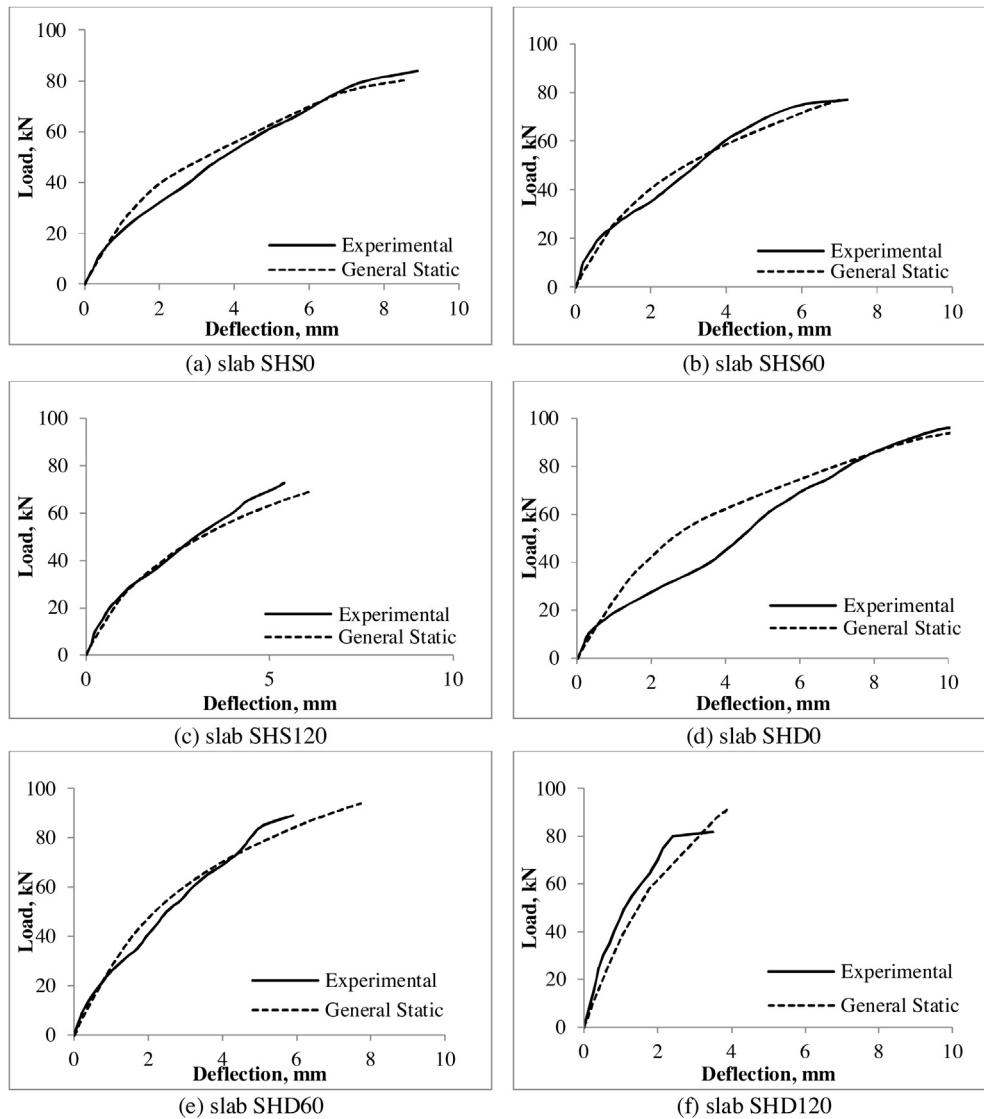(d) slab SHD0

(e) slab SHD60

(f) slab SHD120

**Fig. 19 – Load–central deflection curves using different models.**

cracking patterns with limited exploration of the stress states within the models [22,38]. Here we extend earlier approaches by including predictions of stresses.

The modelling approach taken does not predict discrete cracks and as such is in line with the approach taken by [22]. Figs. 20–22 use the maximum plastic principal strain as a proxy for crack development. These figures show that cracks are predicted numerically in the regions anticipated and also that both the experimental and numerical results are in close agreement for concentric and eccentric cases.

Fig. 20 shows the anticipated cracking for the FE model representing G1 without the shearhead. It can be seen that the crack initiates at the tension side of the slab then propagates inside the slab adjacent to the column in the area of high shear stress until the slab reaches its ultimate capacity at which the punching shear cone is visible. This is in line with critical shear crack theory (CSCT) assumptions [39]. The main basis of the CSCT is that the critical shear crack width is assumed (in two-way spanning slabs) to be proportional to the slab rotation

multiplied by the effective depth of the slab. In CSCT, the crack initiates as a bending crack then the roughness of the crack profile carries the shear force through an inclined concrete compressive strut causing the column to eventually punch through.

Likewise, as shown in Figs. 21 and 22 representing series G2 and G3 (where shearhead reinforcement was embedded), the formation of the crack remains similar to the failure without shear reinforcement, except that the failure occurs at a distance from the shearhead rather than from the column face. As explained, the concrete damage plasticity theory considers the concrete to be cracked after the principal plastic strain exceeds zero, the maximum plastic strain for a cut through the model is shown in Figs. 21 and 22. Observation of the plastic strains show the shearhead increases the failure perimeter.

Figs. 23–25 show the tension face for both experimental and numerical models. The effect of eccentric loading is demonstrating how the slab will tend to crack on only one side. The
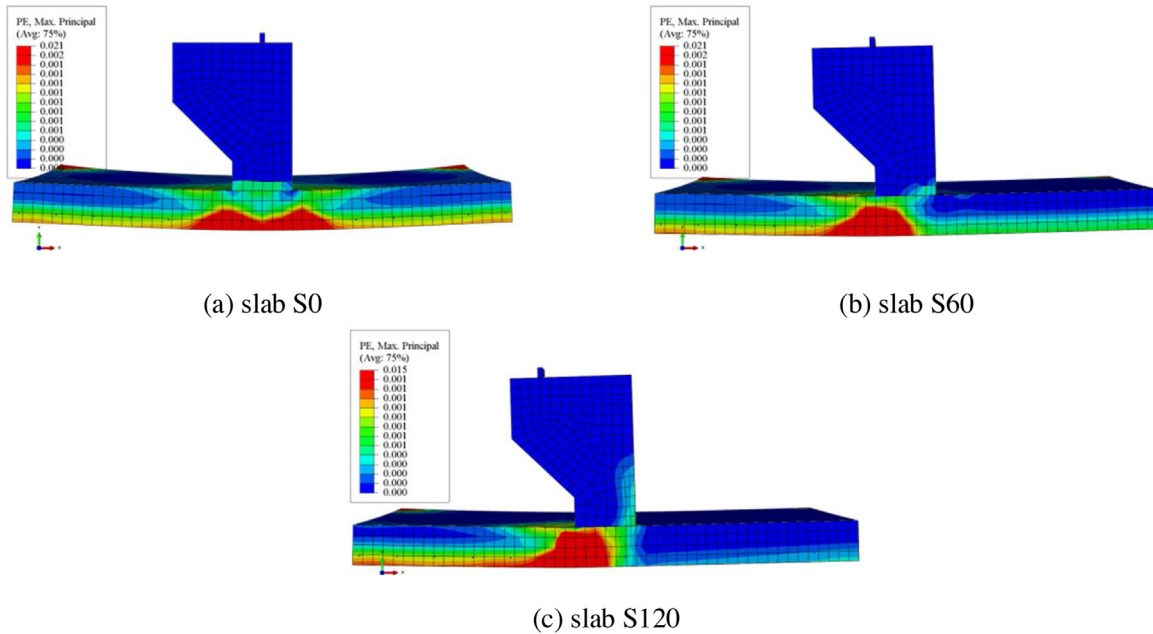
(a) slab S0

(b) slab S60

(c) slab S120

Fig. 20 – Maximum principal strain distribution for G1 at failure.
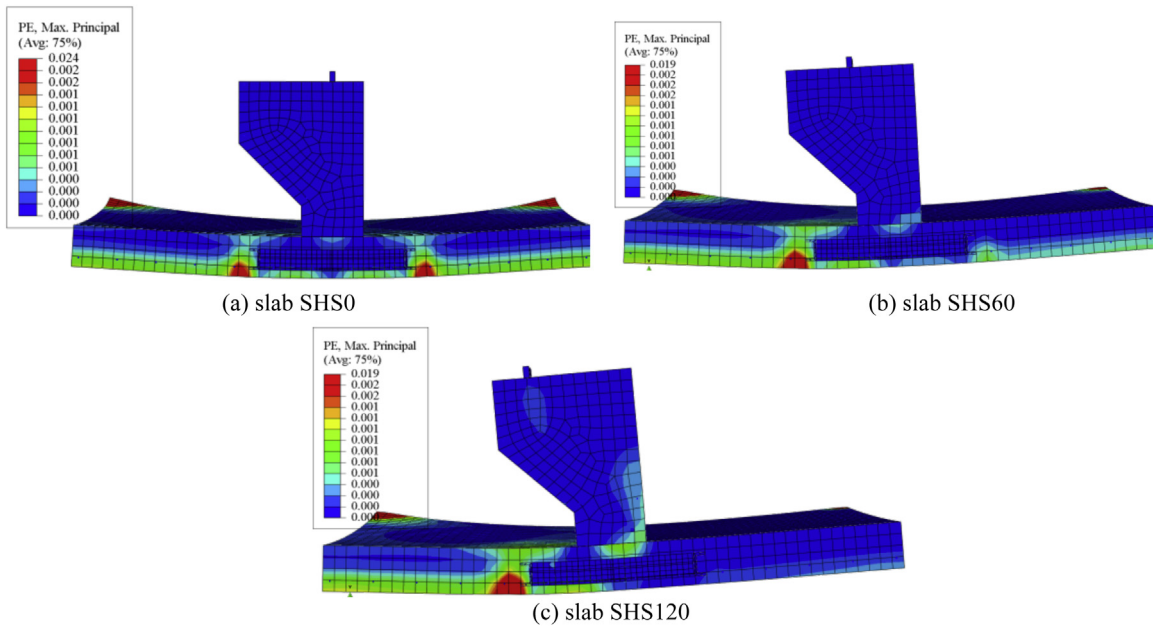


(a) slab SHS0

(b) slab SHS60

(c) slab SHS120

Fig. 21 – Maximum principal strain distribution for G2 at failure.

shearhead reinforcement showed an ability to distribute the shear perimeter away from the column resulting in higher punching shear resistance.

For G1 shown in Fig. 23a, the flexural cracks start to develop near the edge of the column and propagate radially towards the edge of the slab in symmetry until the maximum tensile strength of the concrete is reached causing the slab to fail in symmetrical punching shear in both the test and the FE model. Conversely, as shown in Fig. 23b and c, due to the presence of the eccentric loading the flexural cracks started to develop unevenly resulting in symmetrical punching shear with a low

amount of eccentricity (Fig. 23b) and unsymmetrical punching with a higher amount of eccentricity (Fig. 23c), this is visible in both the experiment and the FE model.

As for G2 and G3, Figs. 21 and 22 show the tension face for both the experimental and numerical models (where the green line on the experimental tension side indicates the position of the shearhead). In both the experiments and FE models, the cracks propagate inside the slab adjacent to the shearhead boundary. Cracks start laterally near the column as flexural cracks and then extend diagonally as the load increases. When the slabs reach their ultimate load capacity the punching shear
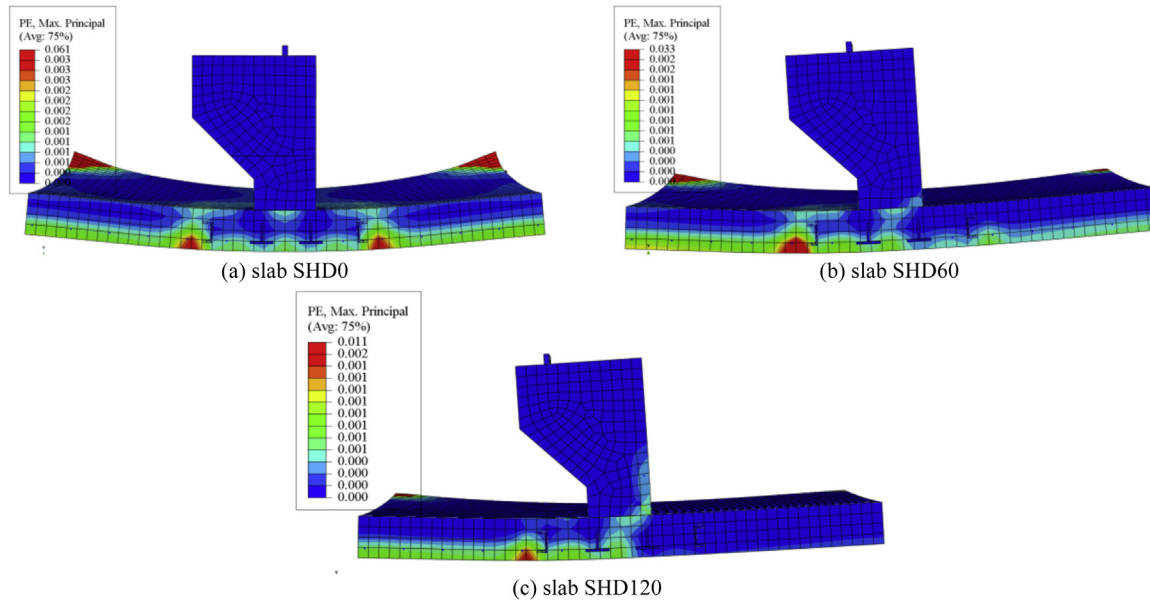
(a) slab SHD0



(b) slab SHD60



(c) slab SHD120

**Fig. 22 – Maximum principal strain distribution for G3 at failure.**

cone is visible due to the sudden opening of the cracks. In the FE models according to the CDP model adopted, cracking initiates when the maximum principal plastic strain is positive [31]. The models with concentric loading show that the slab would fail with symmetrical punching shear. However, the effect of eccentric loading demonstrates how the slab tends to crack on only one side due to the effect of the moment. The numerical models showed that the shearheads could push the shear perimeter away from the column, resulting in a higher punching shear resistance.

From all of the above, it can be seen that the modelling approach at ambient temperature gives close predictions for the load-central deflection, the cracking pattern and the failure mechanism for the slabs with the shearhead.

As for the behaviour of the shearheads embedded within the concrete, the von Mises stress at ultimate load is presented for each case in Fig. 26. From Fig. 26, it can be seen that the overall stresses increase with increasing of eccentricity of the load. However, the stresses in the shearheads nowhere exceed the yield strength of the steel i.e. 540 MPa. This demonstrates that all the slabs failed due to the concrete cracking rather than due to a failure of the shearhead itself.

After demonstrating that the novel shearhead can improve the slab-column connection under both eccentric and concentric loadings, the shearhead model was compared to a numerical model with a larger column with dimensions of 280 mm × 280 mm in place of a shearhead. The model with the larger column failed in punching shear, and the cracking pattern is shown in Fig. 27.

Fig. 28 shows the load-central deflection curve for the new model with a larger column under concentric loading together with both of the slabs with shearheads under concentric loading. This shows that the proposed shearhead system can be as good as enlarging the column size, achieving similar results in an economic and practical way.

## 8.      The effect of fire on the proposed shearhead system

In Section 5, the FE model was described and validated for ambient temperature conditions. In order to validate the numerical model for fire conditions, one of the slabs tested experimentally by Smith [40] is simulated. The slab tested had one central column, the four edges were simply supported. The slab dimensions were 1400× 1400× 75 mm thick and mesh reinforcement was used with 6 mm steel bars having a yield strength of 550 MPa. Two additional bars were placed in each direction on the upper surface to tie the column stub to the slab in accordance with Eurocode 2 [7]. A nominal concrete cover of 16 mm was used. Shear reinforcement was not provided.

Heating was provided in Smith's experiments by radiant panel heaters, with a peak surface temperature of around 380 °C being reached. Surface temperature in this slab was measured (Fig. 29) using thermal couples [40]. This data was used as an input to a numerical thermal analysis that then predicts temperatures at all depths within the slab through time. This thermal field was in turn introduced to the stress analysis model. Only tension reinforcement was present.

Fire loading affects the mechanical properties of concrete under combined heating and loading conditions, which results in the generation of different strain components. Therefore, the best way to understand the deformation of concrete at elevated temperatures is by splitting the total strain into its primary components, as shown in the following equation:

$$\epsilon_T = \epsilon_m + \epsilon_{th} + \epsilon_{lits} + \epsilon_c$$

where $\epsilon_T$ is the total strain, $\epsilon_m$ is the mechanical strain resulting from the mechanical load, $\epsilon_{th}$ is the thermal strain due to the

(a) S0



(b) S60



(c) S120
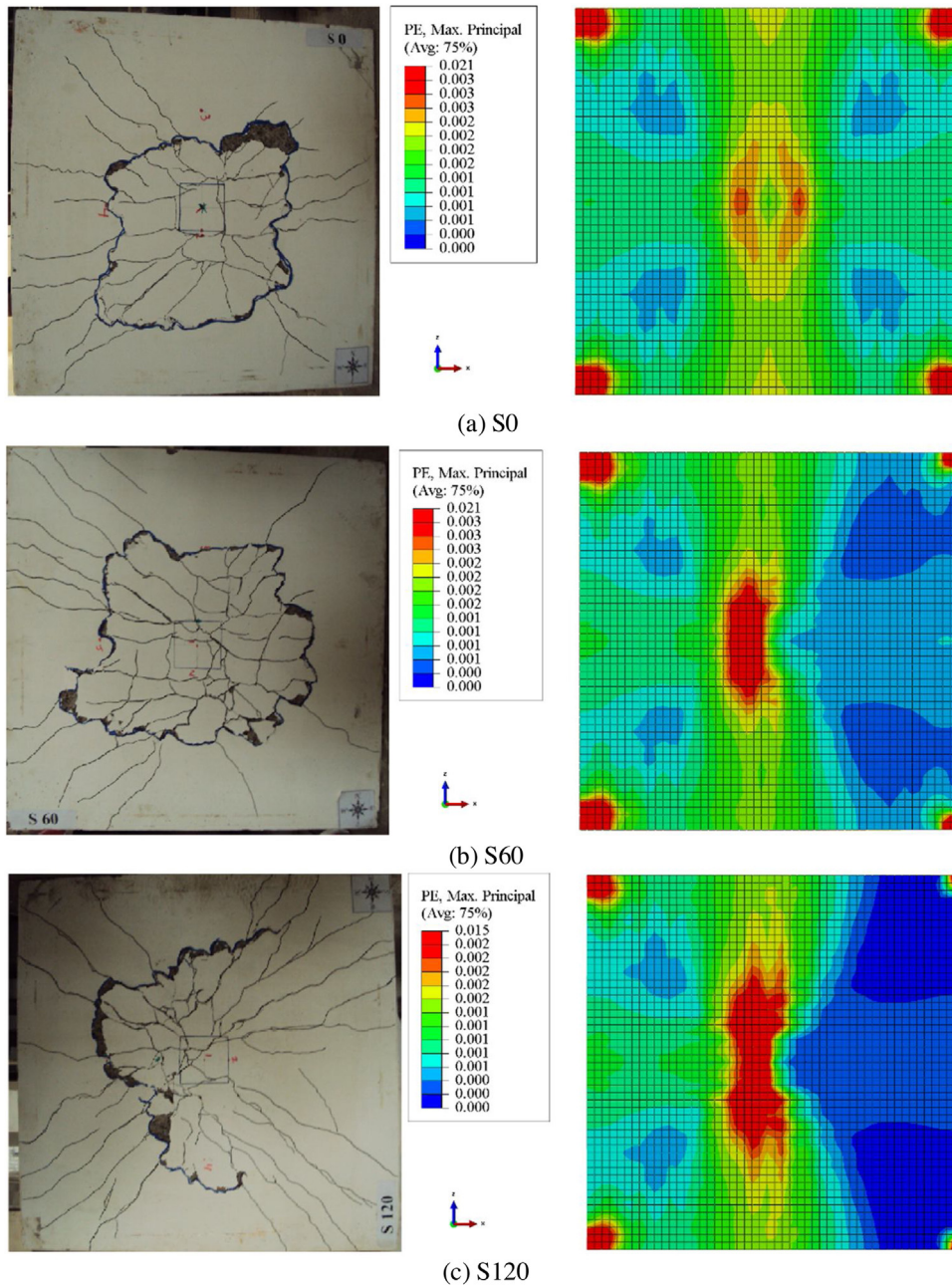
**Fig. 23 – Tension face for both experimental and numerical model for series G1 at failure.**

material expansion, $\varepsilon_{lits}$ is the load-induced thermal strain resulting from the concrete shrinking under a high level of mechanical loading and $\varepsilon_c$ is the creep strain that develops in the material due to external loading over time. The modelling approach adopted by Al Hamd et al. [41,42] gives good results showing a close comparison with experimental data for ambient and elevated temperatures validation (further details on the model can be found in [41,42]).

The same approach was applied to the models with shearhead reinforcement described in the previous section to examine the effect of the shearhead presence in the connection. Fig. 34 shows the effect of embedding the shearheads in the slab and reveals a significant enhancement

for the fire resistance. For an initial study, a heat transfer model slab was developed. The heating profile for this is shown in Fig. 31 and the deflection response shown in Fig. 30 as a first step to generating the thermal profile for the slab without the shearhead. Next, this thermal profile was imported into the concrete part of the mechanical model without shear reinforcement to represent the primary case. A similar procedure was used to develop two models after embedding the shearhead reinforcement in the concrete.

Fig. 32 shows a contour plot of the principal strains in the slab at the end of heating to illustrate the effectiveness of this approach. The classic cone-shaped failure profile of a punching shear failure is clearly visible, as is the effectiveness of the
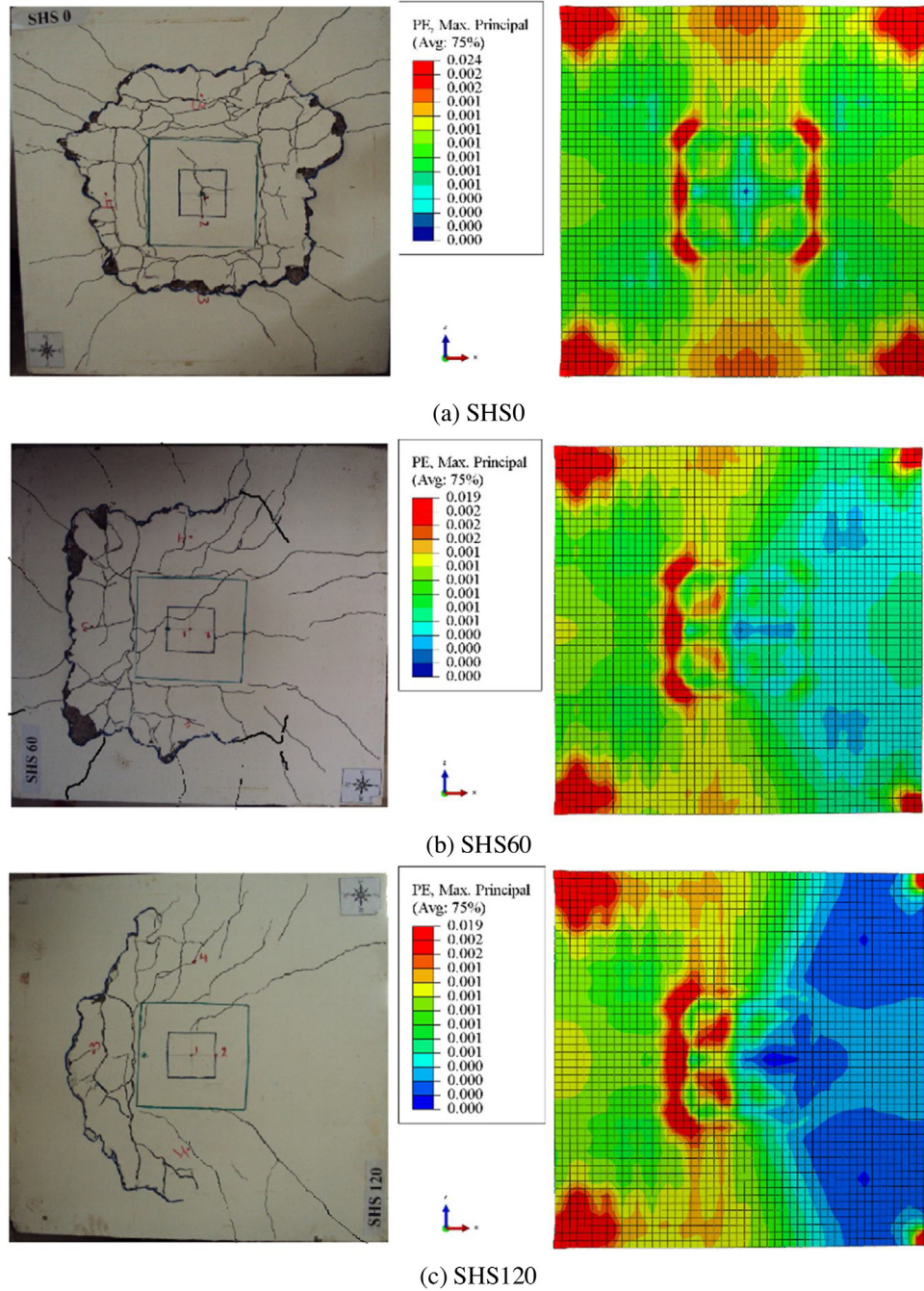
(a) SHS0



(b) SHS60



(c) SHS120

Fig. 24 – Tension face for both experimental and numerical model for G2 at failure.

proposed shear reinforcement, increasing the critical perimeter that resists shear stress in fire.

The stresses in the slab reached the incipient failure stresses through the thickness, the failure profile along with the failure envelope for the slab is shown in Fig. 33 where the assumed crack had travelled across half of the slab. The failure envelope shows the maximum tensile stress that the concrete can sustain at each location, taking into account the temperature profiles and how the concrete material properties vary with temperature. The failure profile shows the maximum principal stresses through the thickness of the slab for the slow-fire scenario (considered along with a path at 45° to the horizontal plane from the column face) [41]. The slab without shear reinforcement resisted heating up to 587 °C and the slabs with shearheads (single and double) resisted heating up to 742 °C and 799 °C, respectively. It can be seen that the existence of the shearheads reduces the compressive stresses developed in the compressive face of the slab due to membrane action, which results in more resistance to the concrete being crushed and a higher punching shear resistance.
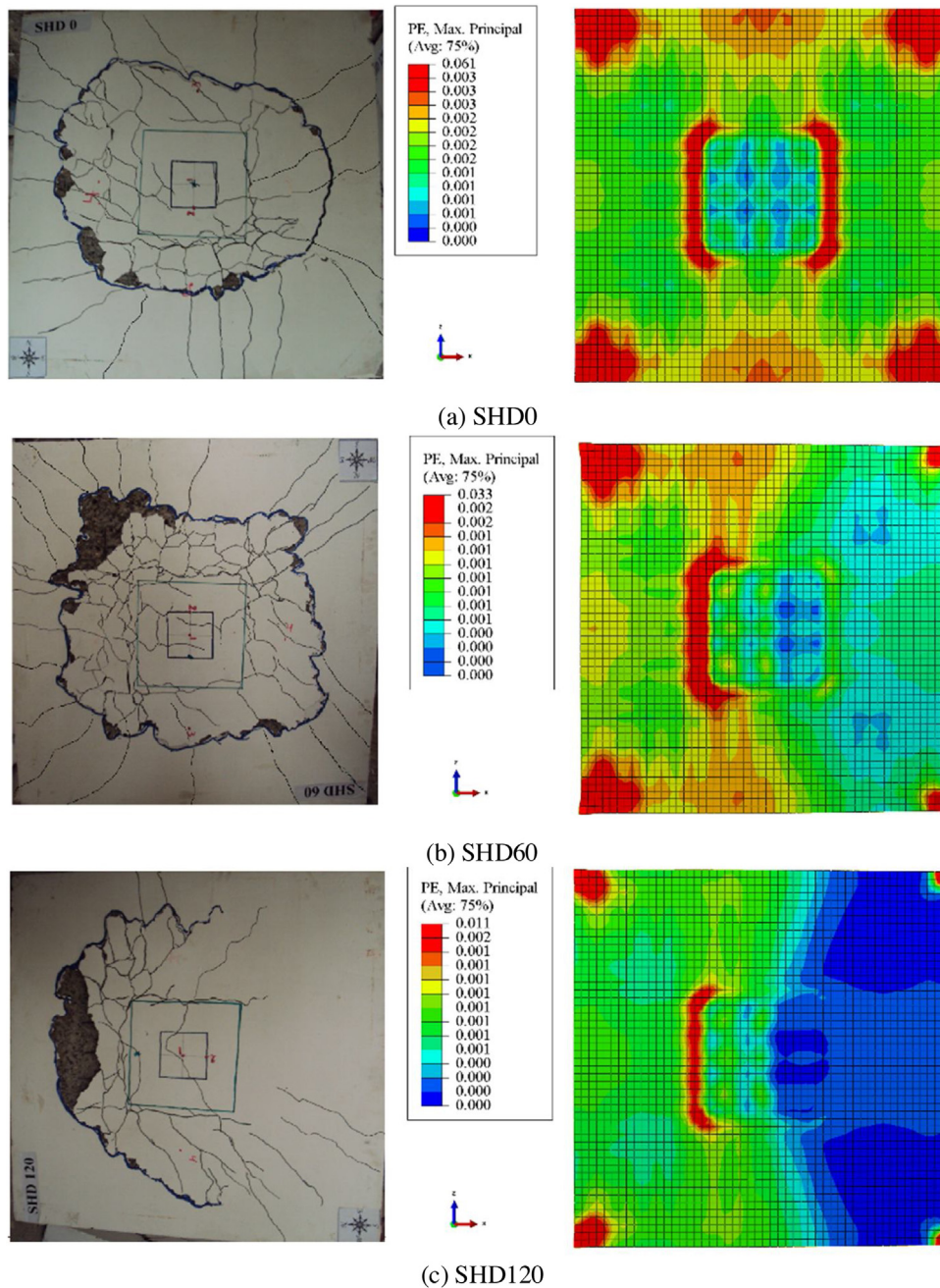
(a) SHD0



(b) SHD60



(c) SHD120

**Fig. 25 – Tension face for both experimental and numerical model for G3 at failure.**

The effect of embedding the shearheads in the slab on the deflection-time/temperature of the slab is shown in Fig. 34, demonstrating significant improvements in fire resistance. The slab with shearhead reinforcement developed more ductility in the fire situation as the stress distribution is different due to the increase in the critical shear perimeter, leading to a higher punching shear resistance.

## 9.    Conclusions

This study has presented experimental and numerical results exploring a novel type of shearhead reinforcement for

connections between concrete flat slabs and columns. Results from nine experimental tests were presented which measured connection behaviour with various degrees of load eccentricity, and two kinds of shearhead design. Next numerical models were validated against these tests and the structural mechanics further explored at ambient temperature. Finally, the effects of heating were introduced to the models to understand how this type of connection might behave in fire. For the scenarios considered in this work, the following conclusions can be drawn:

- The addition of an eccentric load will decrease the ultimate punching shear capacity of slab-column connections. For all
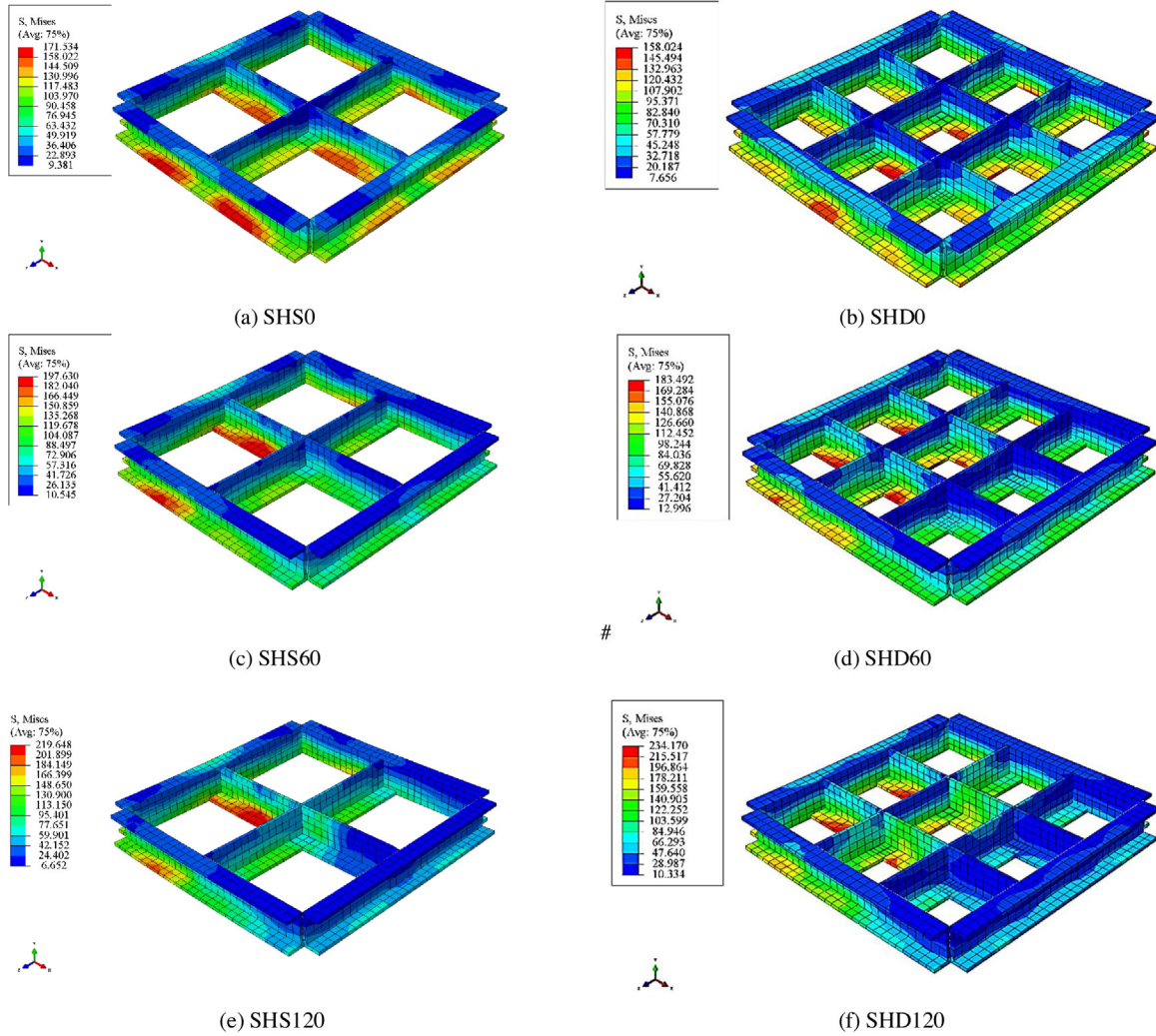
(a) SHS0


(b) SHD0


(c) SHS60


(d) SHD60


(e) SHS120


(f) SHD120

**Fig. 26 – Von Mises stress distribution at ultimate load in the shearheads for G2 and G3 (units in N/mm$^2$).**
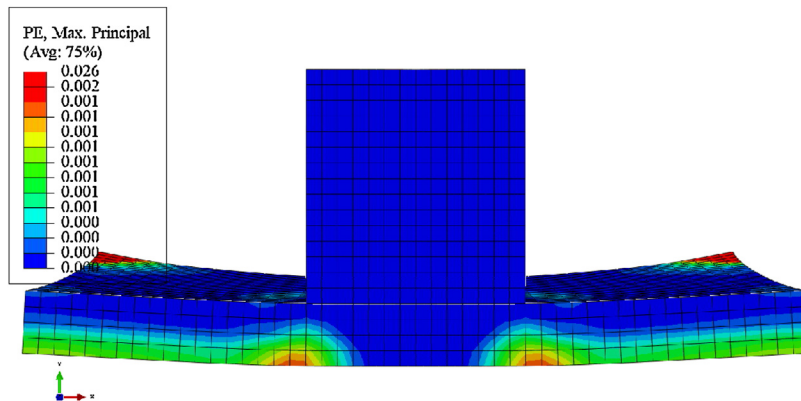


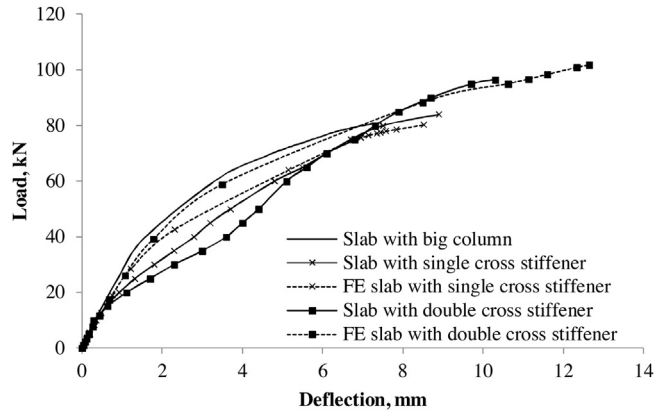**Fig. 27 – Cracking pattern for the assumed column.**

**Fig. 28 – Load–central deflection curve for the model with the enlarged column under concentric loading and both of the slabs with shearheads under concentric loading.**
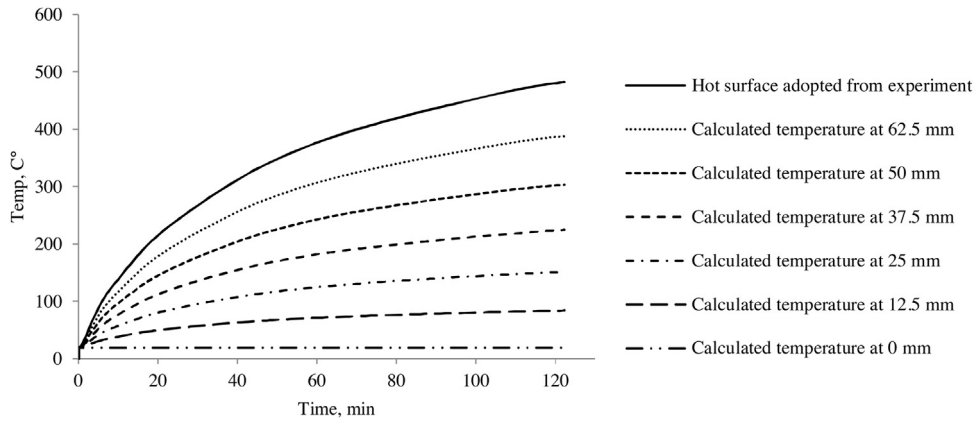


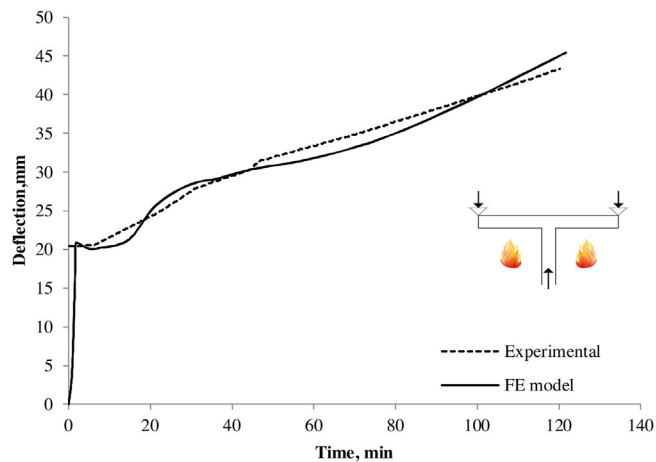**Fig. 29 – Temperature–time data for the heated surface adapted from Smith [40].**



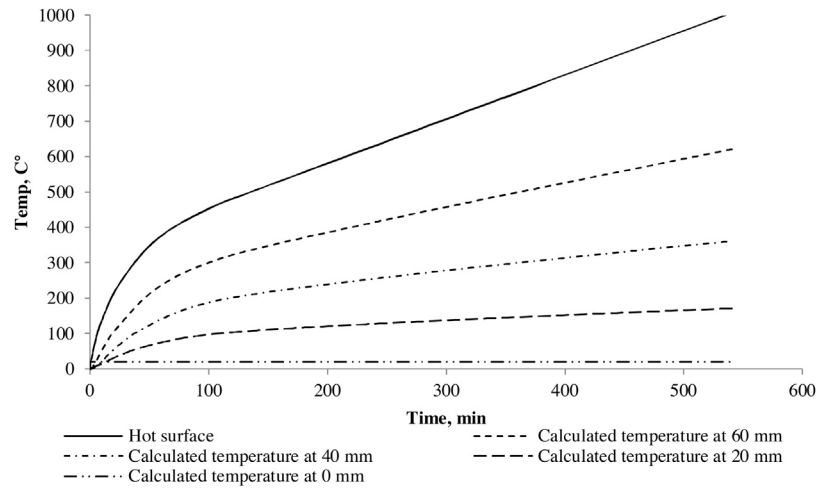**Fig. 30 – Deflection time response for Smith's model[41].**

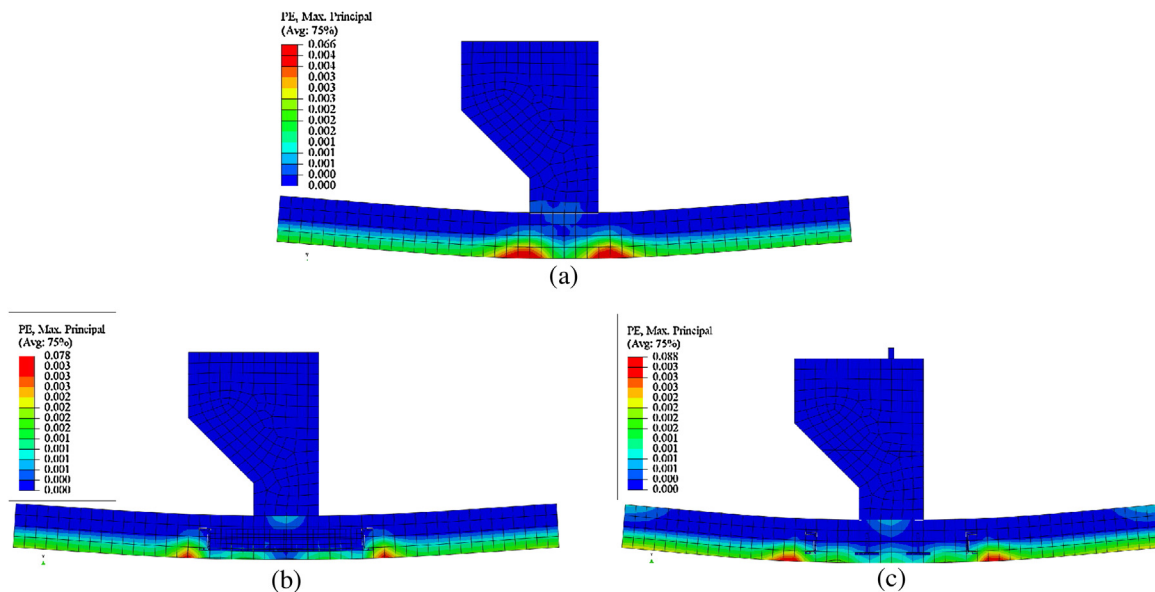**Fig. 31 – Temperature–time data for the heating case.**



**Fig. 32 – Maximum principal strain distribution representing the cracking pattern for the slab for (a) heated slab without shearhead (b) heated slab with single cross stiffener shearhead and (c) heated slab with double cross stiffener shearhead.**

the cases, with and without shearhead reinforcement, this finding is in line with previous work. For cases such as localised heating due to fire, or pattern loading, this loss of capacity may occur on (typically more highly loaded) interior columns and should, therefore, be checked during design.

- The proposed shearhead reinforcement can increase the resistance of the slab-column connections by 15–30% of the ultimate resistance of the connection without shearhead reinforcement. This is achieved by expanding the failure perimeter along which punching shear occurs away from the column, thereby reducing the shear stresses that need to be carried.

- The addition of shearhead reinforcement to the slab-column connection has a similar outcome as increasing the size of the column to create an equivalent shear perimeter. It is thus a more economical and sustainable solution to designing against punching shear.

- Careful numerical modelling can capture punching shear behaviour and the resulting stress states. Such numerical modelling can give a good prediction of punching failure loads for a variety of loading conditions and identify the internal stress states at both ambient and elevated temperature.

- The results suggest that the proposed novel shear reinforcement can resist the effect of fire providing a safer building in an economic way. However, this is based on the currently limited data. Further full-scale experimental work and more realistic fire tests are required to prove the expected behaviour of the shearhead system in real fire situations.
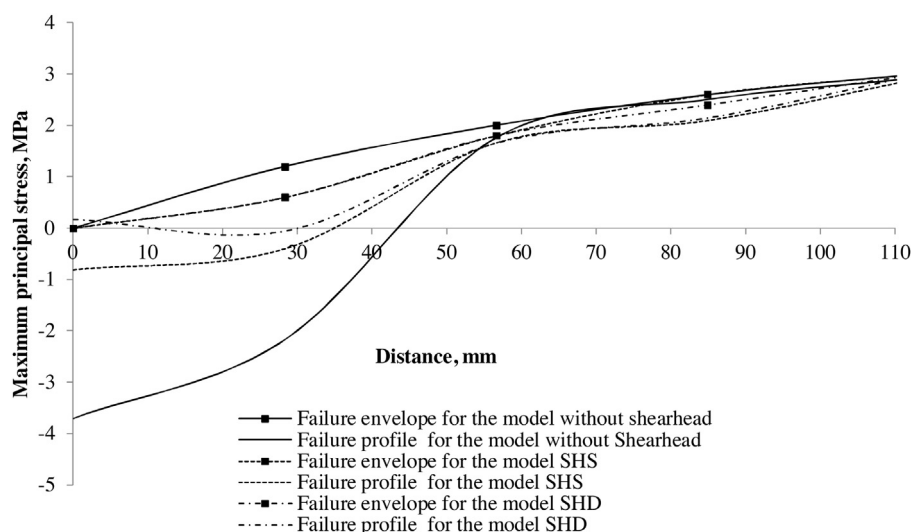
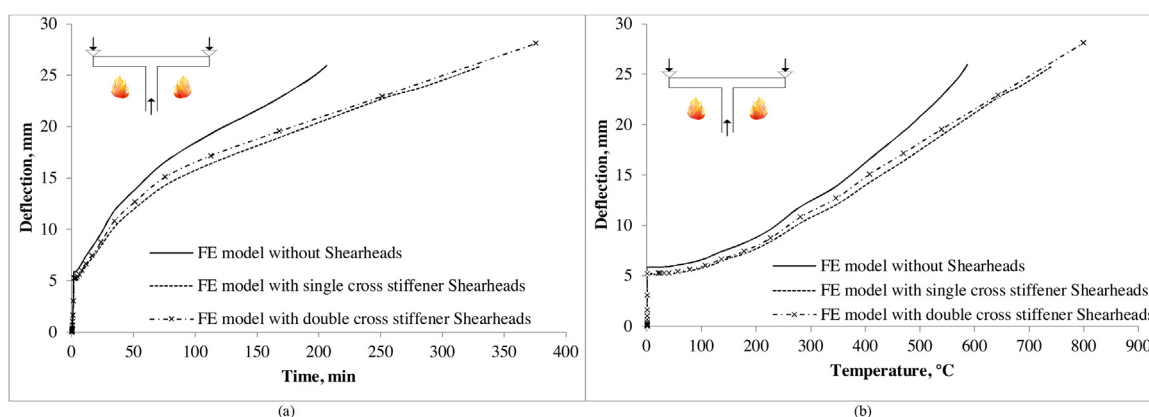**Fig. 33 – Stress state for the heated slab at failure.**



**Fig. 34 – Deflection response against (a) Time and (b) temperature for the slabs with shearhead reinforcement.**

## Conflict of interest

None declared.

## Ethical statement

Authors state that the research was conducted according to ethical standards

## Funding body

## Acknowledgements

REFERENCES

[1] P. Ferguson, J. Breen, J. Jirsa, Reinforced Concrete Fundamental, 3rd ed., John Wiley & Sons, Hoboken, 1988.
[2] S. King, N.J. Delatte, Collapse of 2000 Commonwealth Avenue: Punching Shear Case Study, J. Preformance Constr. Facil. 18 (2004) 54–61.
[3] A.M. Abdullah, Analysis of Repaired/Strengthened R. C. Structures Using Composite Materials: Punching Shear A thesis submitted to The University of Manchester for the degree of Doctor of Philosophy in the Faculty of Engineering and Physical Sciences SCHOOL OF MECHA,. (n.d.).
[4] D.A. Gasparini, M. Asce, Contributions of C. A. P. Turner to Development of Reinforced Concrete Flat Slabs 1905–1909, J. Struct. Eng. 128 (2002) 1243–1252.
[5] R. Park, Reinforced Concrete Structures, 1st ed., John Wiley & Sons, Canada, 1975.

[6] A. Talbot, Reinforced Concrete Wall Footings and Column Footings, Engineering Experiment Station, University of Illinois, Urbana, 1913.

[7] R. Elstner, E. Hognestad, Shearing strength of reinforced concrete slabs, ACI J. Proc. (1956).

[8] J. Moe, Shearing Strength of Reinforced Concrete Slabs and Footings Under Concentrated Loads, Skokie, Illinois, 1961.

[9] M. Ghoreishi, A. Bagchi, M.A. Sultan, Review of the punching shear behavior of concrete flat slabs in ambient and elevated temperature, Struct. Fire Eng. 4 (2013) 259–280.

[10] S. Hamada, Q. Yang, M. Mao, Evaluation of punching shear strength of reinforced concrete slabs based on database, J. Adv. Concr. Technol. 6 (2008) 205–214.

[11] Q. Yang, M. Mao, S. Hamada, Data base for punching shear strength of reinforced concrete slabs and evaluation for CCES equation, Appl. Mech. Mater. 90–93 (2011) 933–939.

[12] N.M. Hawkins, W.G. Corley, Moment Transfer to Columns in Slabs with Shearhead Reinforcement, 1974.

[13] S. Islam, R. Park, Tests on slab-column connections with shear and unbalanced flexure, J. Struc. Div. (1976) 550–568.

[14] S. Islam, R. Park, Tests on Slab-Column Connection with Shear and Unbalanced Flexure, 1975.

[15] S. Megally, A. Ghali, Punching of concrete slabs due to column moment transfer, J. Struct. Eng. 126 (2000) 180–189.

[16] T.H. Kang, M. Asce, J.W. Wallace, K.J. Elwood, Nonlinear Modeling of Flat-Plate Systems (2009) 147–158.

[17] C.L. Moreno, A.M. Sarmento, Punching Shear in Eccenrically Loaded Flat Slabs, in: Challenges Civ. Constr., Torres Marques et al. (Eds), Porto, 2008.

[18] J.-K. Song, J. Kim, H.-B. Song, J.-W. Song, Effective punching shear and moment capacity of flat plate-column connection with shear reinforcements for lateral loading, Int. J. Concr. Struct. Mater. 6 (2012) 19–29.

[19] G. Krüger, O. Burdet, R. Favre, Punching tests on reinforced concrete flat slabs with eccentric loading, in: 2nd Int Ph.D. Symp. Civ. Eng., Budapest, (1998) 1–8.

[20] G. Krueger, O. Burdet, R. Favre, Influence de la rigidité des colonnes sur la résistance au poinçonnement, Lausanne, Switzerland, 1999.

[21] A.C.I. Committee 318, 'Building Code Requirements for Structural Concrete (ACI 318M-11) and Commentary (ACI 318R-11), American C, Farmington Hill, MI, 2011.

[22] A.S. Genikomsou, M.A. Polak, Finite element analysis of punching shear of concrete slabs using damaged plasticity model in ABAQUS, Eng. Struct. 98 (2015) 38–48.

[23] A. Wosatko, J. Pamin, M.A. Polak, Application of damage–plasticity models in finite element analysis of punching shear, Comput. Struct. 151 (2015) 73–85.

[24] B.Q. Abdulrahman, Z. Wu, L.S. Cunningham, Experimental and numerical investigation into strengthening flat slabs at corner columns with externally bonded CFRP, Constr. Build. Mater. 139 (2017) 132–147.

[25] ASTM Standard C39, Specification for Concrete Aggregates, West Conshohocken, PA, 2003, http://dx.doi.org/10.1520/C0039.

[26] ABAQUS, User's Manual, Version 6.13, Dassault Systémes Simulia Corp., Provid. Rhode., 2013.

[27] K. Winkler, F. Stangenberg, Numerical Analysis of Punching Shear Failure of Reinforced Concrete Slabs, in: 2008 Abaqus Users' Conf., 2008, 1–15.

[28] S.J. George, Y. Tian, Structural performance of reinforced concrete flat plate buildings subjected to fire, Int. J. Concr. Struct. Mater. 6 (2012) 111–121.

[29] R. Cook, Finite Element Modeling for Stress Analysis, 1st ed., Jhon Wiley & Sons, Inc., Madison, 1995.

[30] CEB-FIP, Model Code Design of Concrete Structures MC90, Thomas Telford Ltd., London, 1990.

[31] J. Lubliner, J. Oliver, S. Oller, E. Onate, A plastic-damage model for concrete, Int. J. Solids Struct. 25 (1989) 299–326.

[32] J. Lee, G.L. Fenves, Plastic-damage model for cyclic loading of concrete structures, J. Eng. Mech. 124 (1998) 892–900.

[33] Committee E., Eurocode 2: Design of Concrete Structures, Part 1-1: General Rules and Rules for Buildings, 2004.

[34] T. Wang, T. Hsu, Nonlinear finite element analysis of concrete structures using new constitutive models, Comput. Struct. 79 (2001) 2781–2791.

[35] A.S. Genikomsou, M.A. Polak, Finite element analysis of a reinforced concrete slab-column connection using ABAQUS, in: Struct Congr. 2014, 2014, 813–823.

[36] J. Knox, Aspects of Modelling Plain and Reinforced Concrete at Elevated Temperatures, The University of Edinburgh, 2012.

[37] B.H.W. Reinhardt, H.A.W. Cornelissen, D.A. Hordijk, Tensile tests and failure analysis of concrete, J. Struc. Eng. 112 (1986) 2462–2477.

[38] R.B. Gayed, A. Ghali, F. Asce, Unbalanced moment resistance in slab-column joints: analytical assessment, J. Struc. Eng. 134 (2008) 859–864.

[39] A. Muttoni, Punching shear strength of reinforced concrete slabs, ACI Struc. J. 105 (2008) 440–450.

[40] H.K.M. Smith, Punching Shear of Flat Reinforced-Concrete Slabs under Fire Conditions, The University of Edinburgh, 2016.

[41] R.K.S. Al Hamd, M. Gillie, H. Warren, G. Torelli, T. Stratford, Y. Wang, The effect of load-induced thermal strain on flat slab behaviour at elevated temperatures, Fire Saf. J. 97 (2018) 12–18.

[42] R.K.S. Al Hamd, M. Gillie, Y. Wang, Numerical modelling of slab-column concrete connections at elevated temperatures, in: IABSE Conf, Vancouver 2017 Eng. Futur. - Rep., 2017.